

STRUCTURE OF THE EARTH'S CRUST AND UPPER MANTLE
UNDER A PORTION OF CANADIAN SHIELD DEDUCED
FROM TRAVEL-TIMES AND SPECTRAL AMPLITUDES
OF BODY WAVES USING DATA FROM
PROJECT EARLY RISE

by

BEHIC M. GURBUZ

B. Sc., University of Istanbul, 1961
M. Sc., University of British Columbia, 1966

A THESIS SUBMITTED IN PARTIAL
FULFILMENT OF THE REQUIREMENTS FOR THE
DEGREE OF DOCTOR OF PHILOSOPHY

in the Department of Earth Sciences
Division of Geophysics

THE UNIVERSITY OF MANITOBA

October, 1969



ABSTRACT

This study was undertaken in order to determine the velocity-depth function in the Earth's crust and uppermost part of the mantle using travel-times, spectrum amplitude ratios, and relative phase spectra of the reflected, refracted and converted head waves. The interpretation is based on thirty-eight seismic records which were obtained from the "Project Early Rise" experiment during July 1966. The results refer to northwestern Ontario and southeastern Manitoba. A least-square analysis of the travel-time data was made, and the uncertainty of the slope and intercept time was determined. To test the consistency of the velocity distribution obtained from direct, refracted, and converted head waves with the reflected waves, the interval velocities were also determined by using the $T^2 - \Delta^2$ method for the reflected events. Evidence is given for three layers in the Earth's crust, with velocities of 6.1, 6.8, and 7.1 kilometers per second separated by interfaces at average depths 18 ± 2 and 25.5 ± 0.9 kilometers. The velocities in the uppermost part of the mantle were determined as 7.9 and 8.5 kilometers per second representing layering with interfaces at the average depths of 34 ± 1 and 47 ± 1 kilometers respectively. By application of digital data analysis techniques, signal and noise spectra were determined. Also,

the amplitude and phase spectra of each wave type was analysed. The validity of the proposed new model is tested by comparing the observed travel-times, spectral amplitude ratios, and relative phase-shifts with theoretically predicted values. Seismic depth contour maps for the velocity discontinuities were made and a cross-section of the area is also given in the text. The ray-tracing method was also employed to prove the validity of the proposed model from the point-of-view of ray theory.

No refracted waves have been observed from the discontinuities lying above the layers with velocities 6.8 km/sec. and 7.9 km/sec. Even if they exist, it would be impossible to recognize them at distances in excess of 400 kilometers. This has also been proven theoretically by applying the amplitude ratio criteria.

ACKNOWLEDGEMENTS

I wish to thank Dr. D. H. Hall for his valuable discussions during the course of this study. I am also indebted to Dr. K. B. S. Burke for providing many helpful suggestions. I would also like to thank Mr. Z. Hajnal for his interest and assistance during the digitization of the records. I would like to express my sincere thanks to Miss P. Chop for the encouragement and help she has given to me in this study.

During the course of his research, the author was supported by a University of Manitoba Fellowship from the Department of Earth Sciences, University of Manitoba.

This work was financed by a grant to the Department of Earth Sciences by the Arctic Institute of North America and by the National Research Council of Canada.

TABLE OF CONTENTS

		Page
ABSTRACT		i
ACKNOWLEDGEMENT.		iii
LIST OF FIGURES		vii
LIST OF TABLES		x
 CHAPTER		
1	INTRODUCTION	1
	1.1 Symbols Used in Wave Designation	2
2	EXPERIMENTAL SET-UP, INSTRUMENTATION, DIGITIZATION, and SEISMIC RECORDS.	5
	2.1 Experimental Set-up	5
	2.11 Shot location, explosive, shot time schedules, and recording sites	5
	2.2 Instrumentation	8
	2.21 Recording System	8
	2.22 Seismometers	13
	2.23 Time control	16
	2.3 Digitization	16
	2.31 Data acquisition system	16
	2.4 Seismic Records	19
	2.41 Character of seismic records	19
3	THEORETICAL ANALYSIS OF REFRACTED AND REFLECTED WAVES FROM PLANE INTERFACE	22
	3.1 Ray-wave Theory and Assumptions	22

Table of Contents (Continued)

Chapter		Page
3	3.2 Refracted Waves in Layered Media	23
	3.3 Reflected Waves in Layered Media	25
	3.4 Velocity Analysis Using Reflections	27
	3.5 Continuous and Discontinuous Velocity Distribution	30
	3.6 Statistical Analysis of Travel-Time Curves	34
4	THEORY OF REFLECTED AND REFRACTED WAVES . . .	37
	4.1 Introduction	37
	4.2 Basic concepts of the Theoretical Amplitudes of Reflected and Refracted Waves	38
	4.3 Discussion of the Asymptotic Behavior of the Amplitude and Phase Spectra of the Reflected and Refracted Waves	51
	4.4 Amplitude of the Converted Head Waves	52
5	TRAVEL-TIME CURVES OF THE OBSERVED EVENTS, DEPTHS AND CRUSTAL MODELS.	54
	5.1 Determination of the Arrival Times	54
	5.2 Interpretation of the Direct, Refracted, and the Converted Head Waves Travel-Time Curves	54
	5.3 Interpretation of the $T^2 - \Delta^2$ Curves	59
	5.4 Calculations of Depths and Seismic Cross-section	64
	5.5 Crustal Models in the Area	72

Table of Contents (Continued)

Chapter		Page
6	COMPARISON OF THE FOURIER COMPONENT AMPLITUDE RATIOS AND PHASE SPECTRA OF THE OBSERVED EVENTS WITH THE THEORETICALLY PREDICTED VALUES	80
	6.1 Signal Enhancement Technique	80
	6.2 The Fourier Transform of the Digitized Nonperiodic Signal	81
	6.3 Factors Controlling the Observed Amplitudes	84
	6.4 Amplitude Ratios	85
	6.41 Amplitude Ratios	86
	6.42 The P_n/P_m Ratios	87
	6.43 The P_r^m/P^* Ratios	91
	6.44 The P_r^c/PPS Ratios	91
	6.45 The P_r^c/SPS Ratios	97
	6.46 Phase Spectrum P_m, P_r^m, P_r^c Events	101
7	CONCLUSIONS AND SUGGESTIONS	106
	7.1 Suggestions of Future Programs	107
	BIBLIOGRAPHY.	109
	APPENDIX I.	122
	APPENDIX II	126
	APPENDIX III	130
	APPENDIX IV	155

LIST OF FIGURES

FIGURE		PAGE
2.1	Location map for the northwestern Ontario and southeastern Manitoba stations in the Early Rise Experiment 1966. The locations are the center of the array stations	9
2.2	University of Manitoba VLF-2 Refraction System Connection diagram	11
2.3	Frequency response of the VLF-2 refraction system	12
2.4	Seismometer characteristics	15
2.5	Data Acquisition system	17
2.6		
(a)	Records taken at stations from 1 to 10, showing the first and later events	20
(b)	Records taken at stations from 11 to 20, showing the first and later events	21
3.1	Travel-time curve for discontinuous velocity distribution	32
4.1	Schematic diagram of the advancing waves which transmits the energy to the receiver	39
5.1	Reduced travel-time graphs of the first and later events. The least-squares fit (solid lines) satisfy the observed points in the range of 70-80% confidence limits	56
5.2	T^2 versus Δ^2 diagram of the P_r^c events. The least-squares fit (solid line) satisfies the observed points within 80% confidence limits	60
5.3	T^2 versus Δ^2 diagram of the P_r^m events. The least-squares fit (solid line) satisfies the observed points within the 75% confidence limits	61

List of Figures (Continued)

Figure		Page
5.4	T^2 versus Δ^2 diagram of the P_m events. The least-squares fit (solid line) satisfies the observed points within the 90% confidence limits	62
5.5	Depth contours of the top of the layer with velocity of 6.8 km/sec.	68
5.6	Depth contours of the top of the layer with velocity of 7.1 km/sec.	69
5.7	Depth contours of the top of the layer with velocity of 8.5 km/sec.	70
5.8	Cross-section showing the velocity discontinuities interpreted from first and later events across northwestern part of Ontario and southeastern Manitoba.	71
5.9	(a) Correlation between compressional velocity, pressure and rock density.	76
	(b) Observed relation of compressional velocity and density	76
5.10	Ray path diagram	79
6.1	Amplitude (a) and Phase spectrum (b) of the P_n event at the distance 445.4 km. from the shotpoint	88
6.2	Amplitude (a) and Phase spectrum (b) of the P_m event at the distance 731.1 km. from the shotpoint	89
6.3	Comparison of P_n/P_m ratios of the observed events with the P_n/P_m theoretically predicted values	90
6.4	Amplitude (a) and Phase (b) spectrum of the P^* event at the distance 696.3 km. from the shotpoint	92

List of Figures (Continued)

Figure		Page
6.5	Amplitude (a) and Phase (b) spectrum of the P_r^m event at the distance 696.3 km. from the shotpoint.	93
6.6	Comparison of P_r^m/P^* ratios of the observed events with the theoretically predicted values	94
6.7	Amplitude (a) and Phase (b) spectrum of the P_r^c event at the distance 709.0 km. from the shotpoint.	95
6.8	Amplitude (a) and Phase spectrum of the PPS event at the distance 501.7 km. from the shotpoint.	96
6.9	Comparison P_r^c/PPS ratios of the observed events with the theoretically predicted values	98
6.10	Amplitude (a) and Phase (b) spectrum of the SPS event at the distance 501.7 km. from the shotpoint	99
6.11	Comparison of P_r^c/SPS ratios of the observed events with the theoretically predicted values	100
6.12	Phase change of the P_m event as a function of distance from the shotpoint	102
6.13	Phase change of the P^m event as a function of distance from the shotpoint.	103
6.14	Phase change of the P_r^c event as a function of distance from the shotpoint	104

LIST OF TABLES

TABLE		PAGE
2.1	Shot-Time Schedules	6
2.2	Portable VLF-2 Refraction System	8
2.3	Type HS-10-1 Geophone, Model K	13
2.4	Data acquisition system characteristics	18
5.1	Co-ordinates of the recording sites, distances from the source, and the arrival times of the events	55
5.2	The least-squares analysis of the travel-time curves	58
5.3	Crustal Model (From Hall and Hajnal 1969)	74
5.4	Crustal Model (Deduced from Early Rise Data)	75
5.5	Theoretical travel-times and Amplitude ratios of the proposed model	78

CHAPTER I

INTRODUCTION

A programme identified by the code name "Project Early Rise" was initiated by the Advanced Research Project Agency to investigate the Earth's crust and upper mantle under North America, using seismic waves generated by chemical explosions fired in the deep waters of Lake Superior in July 1966.

The Geophysics Division of the University of Manitoba occupied recording sites which were located in the area from latitude 49° to $51^{\circ} 30'$ N., and longitude 92° to 98° W.

In this investigation, the interpretation relies heavily on the deduction of the complete velocity-depth function from the application of theory to the observed travel-times, amplitude ratios and phase shifts of the different types of event. The first stage in the study was the correlation of events which were prominent on the records. In the correlation of the later-arriving events, consideration was given to the travel-times, move-out velocities, and amplitude and phase-shift variations with distance. After distinguishing the nature of the principal events, the next stage of the interpretation was to find the best fit travel time curves for the observed events. For this purpose

the least-squares method was employed and the statistical procedures outlined by Steinhart and Meyer (1961) were used to estimate errors and to establish confidence limits for the derived parameters. Then, the velocity-depth function was determined by applying the Weichert-Herglotz-Bateman integral method to the short-range data given by Hall and Hajnal (1969). To obtain the complete velocity distribution in the Earth's crust, as well as in the uppermost part of the mantle, the long range results were also included in the study. The wide-angle reflection data were used to calculate the interval velocities in the separate media applying $T^2 - \Delta^2$ method.

Seismic depth contour maps have been made for the three velocity discontinuities, found as a result of long range studies, as well as a cross-section. From this information a model was constructed and the theoretically calculated travel-times, amplitude ratios, and the phase shifts for the model were compared with the observed values. This ensured that all prominent events were predicted by the model. The ray paths for reflected and refracted waves were constructed to obtain better understanding of the model and observed data.

1.1 Symbols Used in Wave Designation

It appears from the literature that the designation of wave types is far from standard, and that considerable confusion exists in their definitions. For instance, the

recent report on "Project Early Rise" Warren et al (1967b) defined the P_n event as generally in the range 8.3 to 8.5 km/sec. between about 500 and 1,000 km. from the shot-point. On the other hand, as a result of working on the same project and in the same range, Mereu and Hunter (1969) designated the same type of event by P with apparent velocity of 8.5 km/sec. and called it the upper mantle velocity. The similar event was distinguished by Lehmann (1967) and called P_r . It has also been reported by Meissener (1966) that a refracted or slightly diving event from the uppermost part of Earth's mantle with a velocity 8.5 km/sec. was called P_4 .

To avoid such confusion, it is necessary to explain the symbols which are employed in the present study. They are:

- P_g = Direct wave, travelling in the medium which has a velocity of 6.1 km/sec.
- P_r^c = Reflected wave from the top of the medium with velocity of 6.8 km/sec. and depth of 18 ± 2 km.
- P^* = Refracted wave from the medium which has a velocity of 7.1 km/sec., and average depth of 25.5 ± 0.9 km.
- P_r^m = Reflected wave from the top of the medium with velocity of 7.9 km/sec., average depth of 25.5 ± 0.9 km.
- P_m = Reflected wave from the top of the medium which has a velocity of 8.5 km/sec. at average depth 47 ± 1 km.
- P_n = Refracted wave from the medium with velocity of 8.5 km/sec. at average depth 47 ± 1 km.

In addition to these events, two converted head wave events, PPS and SPS, were observed which come from the medium with a velocity of 6.8 km/sec. and at the average depth 18 ± 2 km.

CHAPTER 2

EXPERIMENTAL SET-UP, INSTRUMENTATION, DIGITIZATION AND SEISMIC RECORDS

2.1 Experimental Set-Up

2.1.1 Shot location, explosives, shot-time schedules, and recording sites.

During the period of 7 to 28 of July, 1966, thirty eight charges, each consisting of 10,650 pounds of DuPont Nitramon WW(EL), were fired at the same site approximately located at lat. $47^{\circ}32.5'$ N., long. $88^{\circ}55.20'$ W., and water depth of 110 fathoms.

With minor changes in daily shooting schedules, plus shot times, two shots were fired at 0330 and 0430 E.S.T. on each of the 20 working days, except July 7 and July 26, 1966. The detailed information about the shot times and locations are given in Table 2.1.

The seismic waves generated by the explosions were recorded by about a dozen U. S. and Canadian participating groups at progressively increasing distances along lines radiating away from the source. A four-man crew of the Geophysics division of the University of Manitoba performed the tasks necessary to record the signal at 20 sites in the northwestern

Table 2.1

(From Technical Letter No. 6, Project Early Rise, 1967)

Shot No.	Date July 1966	Eastern Standard Time			Shot Locations	
		Hr.	Min.	Sec.	Latitude, N.	Longitude, W
1	7	05	00	00.05	47°32.56'	88°53.85'
2	8	03	30	00.02	47°32.67'	88°56.57'
3	8	04	30	00.01	47°32.67'	88°56.35'
4	9	03	30	00.04	47°32.95'	88°56.30'
5	9	04	30	00.05	47°32.98'	88°56.35'
6	10	03	30	00.02	47°33.09'	88°56.35'
7	10	04	30	00.01	47°33.03'	88°56.34'
8	11	03	30	00.04	47°33.08'	88°56.06'
9	11	04	30	00.04	47°33.08'	88°56.05'
10	12	03	30	00.04	47°33.19'	88°56.40'
11	12	04	30	00.04	47°32.95'	88°56.27'
12	13	03	30	00.04	47°32.37'	88°56.54'
13	13	04	30	00.04	47°32.32'	88°56.42'
14	14	03	30	00.03	47°33.20'	88°56.48'
15	14	04	30	00.04	47°32.78'	88°56.53'
16	15	03.	30	00.04	47°33.14'	88°56.43'
17	15	04	30	00.05	47°32.97'	88°56.28'
18	18	04	00	00.03	47°32.97'	88°56.15'
19	18	05	00	00.00	47°33.02'	88°56.31'
20	19	03	30	00.01	47°33.08'	88°56.80'
21	19	04	30	00.04	47°32.88'	88°56.79'

Table 2.1 (Continued)

Shot No.	Date July 1966	Eastern Standard Time			Shot Locations	
		Hr.	Min.	Sec.	Latitude, N.	Longitude, W
22	20	03	30	00.04	47°32.94'	88°56.00'
23	20	04	30	00.03	47°32.92'	88°55.93'
24	21	03	30	00.04	47°33.20'	88°56.49'
25	21	04	30	00.04	47°33.28'	88°56.33'
26	22	03	30	00.03	47°33.29'	88°56.29'
27	22	04	30	00.03	47°33.29'	88°56.32'
28	23	03	30	00.03	47°33.07'	88°56.21'
29	23	04	30	00.04	47°33.05'	88°56.13'
30	24	03	30	00.03	47°33.12'	88°56.67'
31	24	04	30	00.02	47°33.19'	88°56.59'
32	25	03	30	00.02	47°33.23'	88°56.60'
33	25	04	30	00.02	47°33.16'	88°56.02'
34	26	MISFIRE			MISFIRE	
35	26	04	30	00.02	47°32.88'	88°56.27'
36	27	03	30	00.02	47°33.23'	88°57.10'
37	27	04	30	00.02	47°33.16'	88°56.73'
38	28	03	30	00.01	47°32.91'	88°56.14'
39	28	04	30	00.02	47°32.77'	88°56.08'

Ontario and southeastern Manitoba. Distances from the source ranged from 426 to 775 km. The exact location of the recording sites are shown in figure 2.1. All of the shots were primed and located by a U. S. Navy demolition crew working on the shooting vessel, the U. S. Coast Guard Cutter Woodrush.

2.2 Instrumentation

2.21 Recording System

The detection and recording of the signals were carried out with a mobile unit which consists of low frequency equipment (Texas Instrument VLF-2 with bandpass 0.5 c.p.s. to a high cut-off frequency selected in the range of 8 to 48 c.p.s.), and a 14-channel FM analog tape-recording unit. The specifications are given in Table 2.2.

Table 2.2

Portable VLF-2 Refraction System

Specifications (Supplied by the Manufacturer)

<u>Sensitivity:</u>	1" p-p galvanometer deflection
(given for 23 ohm	for 1 microvolt input with input
galvanometer having	transformer coils at 1000 henry
1" p-p deflection for	inductance.
1.5 mv steady state	2" p-p galvanometer deflection
sensitivity.)	for 1 microvolt input with input
	transformer coils paralalled for
	250 henry inductance.

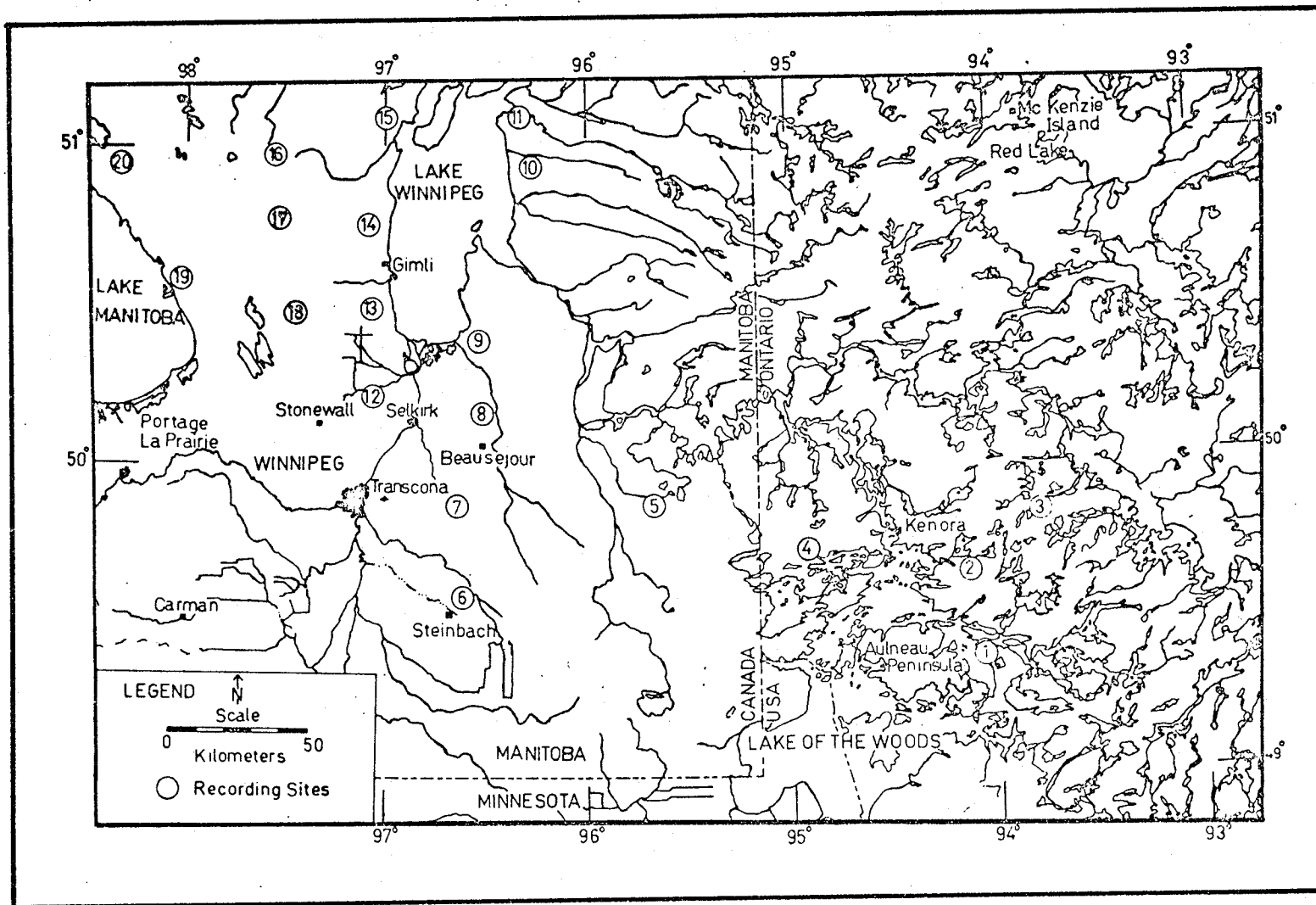


Figure 2.1 Location map for the northwestern Ontario and southeastern Manitoba stations in the Early Rise experiment of 1966. The locations are the center of the array stations.

Table 2.2 (Continued)

<u>Input Noise:</u>	0.3 microvolts RMS
<u>Frequency Response:</u>	1 to 40 cps
<u>Input Impedance:</u>	10K in parallel with the primary of 1000 (or 250) henry transformer.

Output

Camera:	Dual outputs with 4:1 amplitude ratio with source resistance of 47 ohms.
Recorder:	Delivers .5, .7, 1, 1.5, 2.3, or 3 ma RMS to 60 ohms. Direct recorder magnetic head and .9 volts RMS to FM modulator.

Figure 2.2 is a simplified connection diagram of the VLF-2 system.

Figure 2.3 shows the frequency response of the VLF-2 system, including the camera unit. During the test the attenuation setting was 60 db. and the input was constant. The frequencies marked on the curves indicate frequency filter settings. The attenuation controls were checked and they attenuate in 6 db. steps. The galvanometers^a have a flat frequency-response curve through the frequency range, and therefore their effect on the recording camera is only to alter the amplitude by a constant factor which can be easily determined.

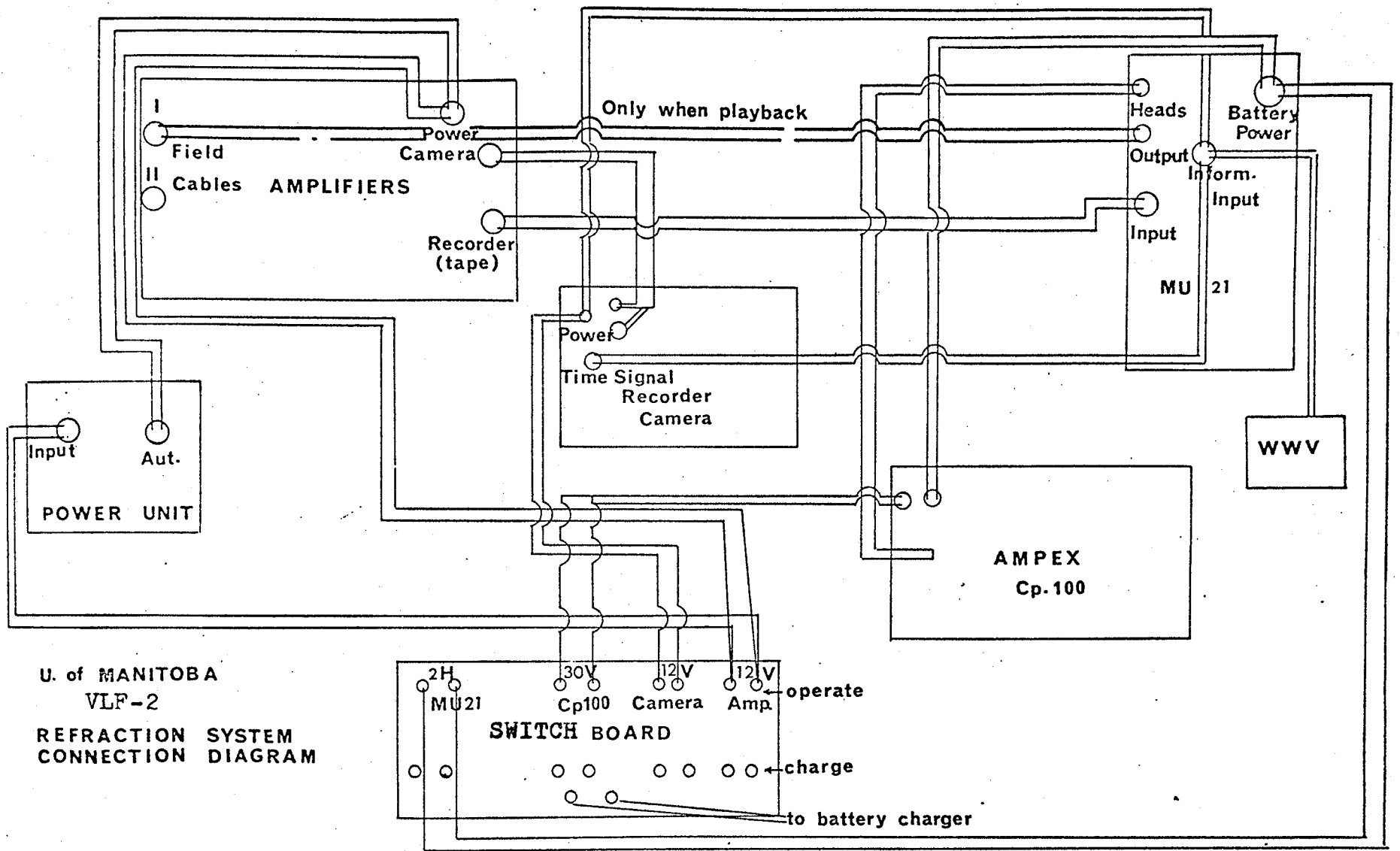


FIGURE 2.2

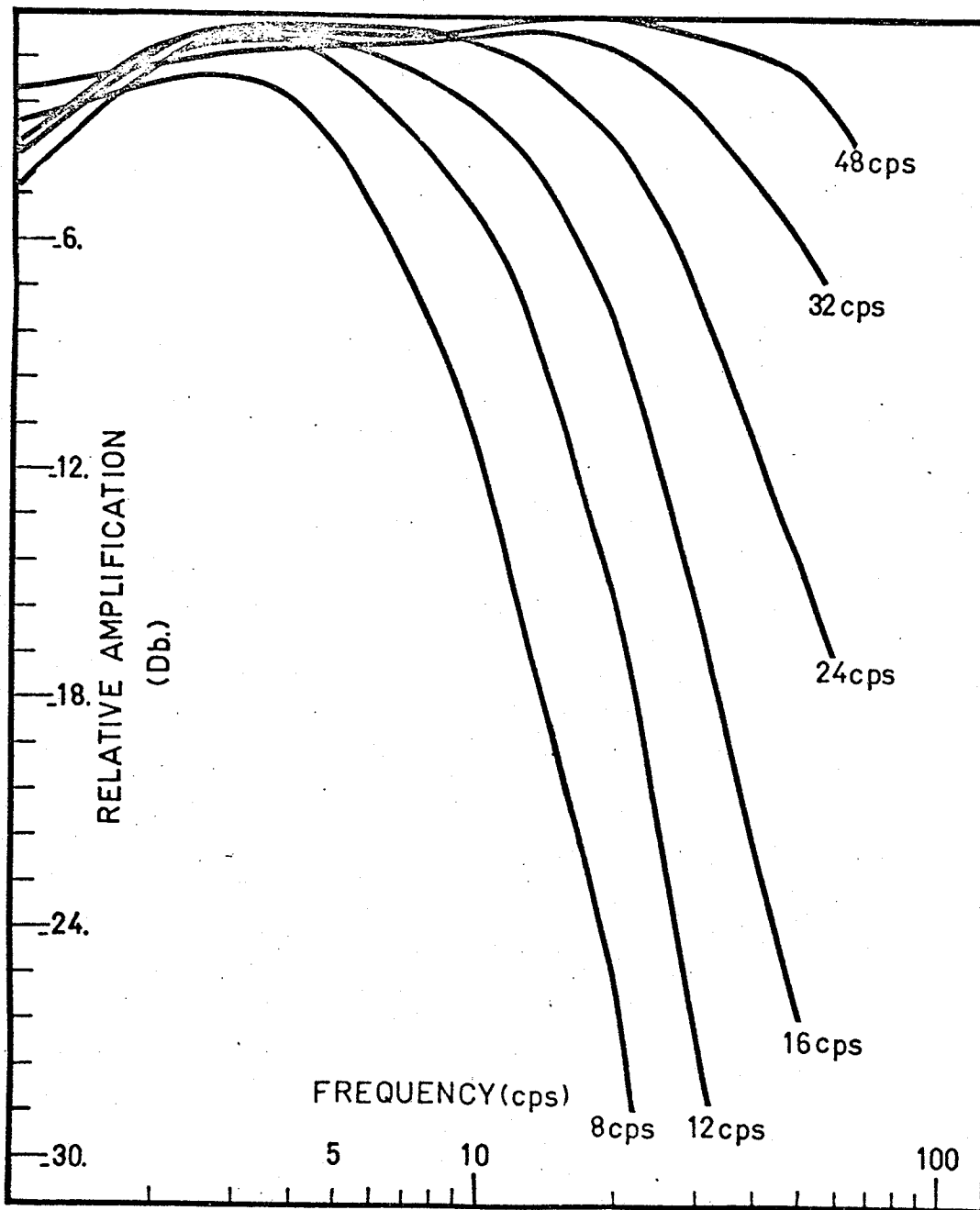


Figure 2.3 Frequency response of the VLF-2 refraction system.

2.22 Seismometers

During this survey, HS-10-1 type of seismometers were employed having high output velocity sensitivity with a natural frequency of 1 c.p.s. and connected singly, one to a trace. Calibration data supplied by the manufacturer is shown in Table 2.3.

Table 2.3

Type HS-10-1 Geophone, Model K

Specifications

Frequency (at 5-10 mv.)	1 cps
Frequency Limits at 0.1 cps	0.9 to 1.1 cps
DC Resistance (DCR) at 25 ^o C	390 ohms
DCR Limits at 5%	371 to 409 ohms
Number of turns	5000 total
Wire size and type	No. 30,ss
Mean Length of turn (MLT)	0.716 foot
Length of wire	3580 feet
Intrinsic Voltage Sensitivity (G)	2.6v/in/sec. (vis)
Open Circuit Damping (Bo)	28%
Open Circuit Damping Limits at 10%	25.2% to 30.8%
Open Circuit Overswing Ratio	10/4.45 to 10/3.64
Coil form weight, bare (incl. all weight rings)	391 grams
Coil form weight, processed	392 grams
Copper weight	505.5 grams